

## Journal Pre-proofs

Effect of additives in the nucleation and growth of methane hydrates confined in a high-surface area activated carbon material

C. Cuadrado-Collados, J. Farrando-Pérez, M. Martínez-Escandell, A. Missyul, J. Silvestre-Albero

PII: S1385-8947(20)30215-1  
DOI: <https://doi.org/10.1016/j.cej.2020.124224>  
Reference: CEJ 124224

To appear in: *Chemical Engineering Journal*

Received Date: 25 November 2019  
Revised Date: 21 January 2020  
Accepted Date: 24 January 2020

Please cite this article as: C. Cuadrado-Collados, J. Farrando-Pérez, M. Martínez-Escandell, A. Missyul, J. Silvestre-Albero, Effect of additives in the nucleation and growth of methane hydrates confined in a high-surface area activated carbon material, *Chemical Engineering Journal* (2020), doi: <https://doi.org/10.1016/j.cej.2020.124224>

This is a PDF file of an article that has undergone enhancements after acceptance, such as the addition of a cover page and metadata, and formatting for readability, but it is not yet the definitive version of record. This version will undergo additional copyediting, typesetting and review before it is published in its final form, but we are providing this version to give early visibility of the article. Please note that, during the production process, errors may be discovered which could affect the content, and all legal disclaimers that apply to the journal pertain.

© 2020 Elsevier B.V. All rights reserved.



## Effect of additives in the nucleation and growth of methane hydrates confined in a high-surface area activated carbon material

C. Cuadrado-Collados<sup>1,\*</sup>, J. Farrando-Pérez,<sup>1</sup> M. Martínez-Escandell,<sup>1</sup> A. Missyul,<sup>2</sup> J. Silvestre-Albero<sup>1,\*</sup>

<sup>1</sup>Laboratorio de Materiales Avanzados, Departamento de Química Inorgánica-IUMA, Universidad de Alicante, Spain

<sup>2</sup>CELLS-ALBA Synchrotron, Cerdanyola del Vallés, Spain

A high-surface area activated carbon material (PPAC) prepared from a petroleum residue has been used as a host structure to promote the nucleation and growth of confined methane hydrates after the incorporation of additives. Sodium dodecyl sulfate (SDS), Leucine and Tetrahydrofuran (THF) have been evaluated either dissolved in the pre-impregnation media (ultrapure water) or incorporated in the carbon surface using a mechanochemical approach. High-pressure methane adsorption isotherms show that the mechanochemical approach does not improve the storage performance of the original carbon material due to the steric effects by the bulkier organic functionalities. Furthermore, the incorporation of the additives shifts the nucleation in narrow pores to higher pressures.

On the contrary, when the additives are dissolved in water, high-pressure methane isotherms anticipate a modification in the kinetics and/or thermodynamics of the nucleation process. Whereas gas hydrates grown in large pores and/or the external surface exhibits a significant reduction in the induction time, the nucleation process in narrow micropores becomes more uniform and occurs in a narrower pressure window, slightly shifted to higher pressures. However, no changes in the total uptake at 10 MPa could be found. The situation is different when THF is dissolved in water. In this case, the nucleation takes place at pressures below the natural process (< 3-4 MPa), the total amount of methane stored at 10 MPa being slightly limited. In-situ synchrotron X-ray diffraction studies anticipate a SI structure for the pure water methane hydrates, while a combination of SI and SII is identified for the THF-based system.

### 1. Introduction

Nowadays, natural gas storage in the transportation sector is mainly based on compressed (CNG) and liquefied (LNG) technologies, working at room temperature and high pressure (25 MPa) or at cryogenic temperatures and atmospheric pressure, respectively. Both technologies still present several drawbacks and risks associated with their high cost and safety issues that must be minimized [1,2]. An alternative approach to storage natural gas (or methane, its main component) constitutes the adsorption of these

probes in porous materials [3-5]. By taking advantage of the large adsorption potential in narrow pores, nanoporous materials can store a large amount of gas, with a high packing density, and under mild pressure and temperature conditions [6]. However, actual storage values in porous solids, mainly metal-organic frameworks and activated carbon materials, exhibit certain limitations, at least in a gravimetric basis, to fulfil the new methane targets defined by the US Department of Energy (see DOE MOVE program at [https://arpa-e.energy.gov/sites/default/files/documents/files/MOVE\\_ProgramOverview.pdf](https://arpa-e.energy.gov/sites/default/files/documents/files/MOVE_ProgramOverview.pdf)). Only very exceptional materials can reach these numbers to date, although restricted to volumetric basis [5, 7-9].

In nature, methane is also found entrapped in crystalline solids, the so-called methane hydrates. These compounds are formed when methane and water come in contact under thermodynamically favorable conditions, i.e. high pressure and relatively low temperature, giving rise to an ice-like hydrogen-bonded crystalline structure. Under these conditions, natural hydrates crystallize in a cubic structure known as type sl. The unit cell of this structure is constituted by cages of two different types: (i) six large cages having 12 pentagonal and 2 hexagonal faces (denoted by  $5^{12}6^2$ ) formed by 24 water molecules and (ii) two small cages having 12 pentagonal faces (denoted by  $5^{12}$ ) formed by 20 water molecules; resulting in a nominal stoichiometry  $1\text{CH}_4 : 5.75 \text{H}_2\text{O}$  [10].

These compounds constitute a potential energy source since 1 liter of methane hydrate can store up to 164 liters of methane gas. Thus, the development of artificial methane hydrates as fuel storage media may be considered as a promising alternative to CNG and LNG, provided that these artificial hydrates can be developed under milder conditions than in nature and, the most important aspect, with much faster kinetics. In this context, in the last decade many research groups have investigated the formation of methane hydrates at laboratory scale [11-13]. In nature, methane hydrate formation is a long geological process that took place slowly throughout hundreds of years. Formation of artificial methane hydrates in bulk phase was also found to be a very slow process, the associated yield (water-to-hydrate conversion) being rather low. This observation is very reasonable since hydrates nucleation and growth takes place at the gas-liquid interphase. The limited interfacial area in conventional reactors and the low solubility of  $\text{CH}_4$  in water, limits the gas hydrate nucleation process to the interfacial water layer [14]. Furthermore, gas hydrates already grown at the gas-liquid interphase act as a barrier, thus blocking further conversion of bulk water-to-hydrate. Therefore, only a small volume of liquid is prone to form hydrates while the rest of bulk water keeps free of  $\text{CH}_4$  without any conversion.

Different methods have been proposed in the literature in order to enhance the solubility of hydrocarbons into water. For instance, Kim et al. reduced the induction time for the nucleation of the hydrates and

increased the hydrate yield by incorporating mechanical agitation into the system [15]. Nevertheless, the energetic cost associated to the agitation is too high and other alternatives must be considered to promote the hydrate formation. A potential alternative constitutes the use of additives, dissolved in water, able to alter/modify the methane hydrate formation/dissociation processes [16]. Additives can be classified in two groups: kinetic and thermodynamic hydrate promoters. The formers have been widely applied to increase the kinetics of the bulk water-to-hydrate conversion [17, 18]. Zhong et al. observed that the addition of SDS (242 ppm) enhances the hydrate formation rate at 3.89 MPa and 275.2°C in a quiescent system by a factor greater than 700, compared to pure water [19]. Similarly, Veluswamy et al. observed that the addition of leucine to water raised the hydrate yield from 12% to 81% at 275.2 K and 10 MPa [20]. It is widely accepted that in the presence of these additives, solubility of hydrocarbons is highly enhanced so that more CH<sub>4</sub> is prone to interact with water molecules to form the corresponding hydrates. The second group of hydrate promoters have the ability to modify the thermodynamics (hydrate phase stability), so that these hydrates can be synthesized under milder temperature and pressure conditions [21, 22]. Under these circumstances, it is possible to form new hydrate structures (thermodynamic promoters usually participate in the crystal structure) with better stability compared to the traditional sI structure found in pure water methane hydrates [16,23]. Generally, these promoters are bulkier hydrocarbons such as tetrahydrofuran (THF) or cyclopentane. Kumar et al. evaluated the hydrate formation in a THF-water solution under high pressure methane [22]. Powder X-ray diffraction studies of the synthesized hydrates confirmed the presence of a sII structure with THF occupying the large cages while the small ones remain occupied by CH<sub>4</sub> molecules. These mixed CH<sub>4</sub>-THF hydrates were proved to be stable at near atmospheric pressure for more than 2 months.

Another alternative to modify the thermodynamics and kinetics of the methane hydrate formation process concerns the addition of nanoporous materials in the synthesis media. By taking advantage of the confinement effects in the inner pores of these solids, methane hydrate formation can be promoted under milder pressure and temperature conditions, and the most important, with faster kinetics than natural or bulk hydrates. Previous studies from our research group have shown that activated carbon materials obtained from petroleum pitch and using KOH as activating agent constitute the most promising candidates reported so far to this end [24, 25]. These activated carbon materials combine a proper development of porosity and a proper hydrophobicity to promote the preferential nucleation and growth of these confined hydrates, with a nearly 4-fold increase in the methane storage capacity compared to

the dry material. On the contrary, nanoporous solids with a larger hydrophilicity (MOFs or zeolites) does not succeed to achieve these excellent values [26, 27].

A potential approach to improve these numbers in activated carbon materials could be the use of additives, either dissolved in water or anchored in the carbon surface. To our knowledge, no studies have been reported in the literature so far concerning the effect of additives in confined nanospace. With this in mind, the main goal of this manuscript is the evaluation of the methane hydrate formation process in a high-surface area petroleum-pitch activated carbon material (PPAC) before and after the modification with additives. To this end, two different approaches will be evaluated: (a) the mechanochemical modification of the carbon surface with the additives and (b) the incorporation of the additives dissolved in water. Sodium dodecyl sulfate (SDS), leucine and tetrahydrofuran (THF) were selected for this study.

## 2. Experimental section

A high-surface area activated carbon (PPAC) was prepared from a petroleum pitch as a carbon precursor and using a conventional chemical activation route with KOH. A detailed description of the synthesis process can be found elsewhere [25]. Briefly, the synthesis involves the activation of the pyrolyzed petroleum pitch with potassium hydroxide (KOH) (KOH: carbon precursor ratio of 6:1) at 800°C for 2h under a nitrogen flow (50 ml/min), followed by a washing step using HCl and H<sub>2</sub>O until complete removal of the chemical agent (neutral pH).

As mentioned above, the additives selected for this study were leucine, sodium dodecyl sulfate (SDS) and tetrahydrofuran (THF) (Table 1). The solid additives (leucine and SDS) were introduced into the activated carbon following two different approaches:

a) Mechanochemical approach: In the first approach both compounds (activated carbon and additives) were finely grounded in a ball mill for 30 min at 150 rpm, resulting in a homogeneous fine mixture. Finally, the powder was washed with abundant distilled water to remove the excess of the additive and dried overnight at 75°C. At this point it is important to highlight that a similar ball milling was applied to the original activated carbon, but in the absence of additives. Samples are labeled PPAC, PPAC@Leucine and PPAC@SDS.

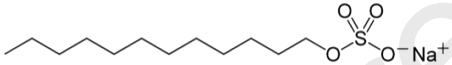
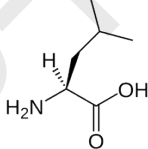
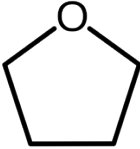
b) Impregnation approach: The second approach consisted in preparing an aqueous solution of the additive by using a magnetic stirrer (see Table 1 for further details). Afterwards, the activated carbon PPAC

was directly impregnated with the solution to a final ratio of  $R_w = 4.1 \text{ g}_{\text{H}_2\text{O}}/\text{g}_{\text{AC}}$  (oversaturation conditions). The obtained samples are labeled PPAC + Leucine and PPAC + SDS.

In the first approach, the main objective was to promote the anchoring of the additive to the carbon surface by taking advantage of the energy released during the ball-milling process, while in the second approach the additive was solubilized in ultrapure water. For THF as additive, the incorporation was done using exclusively the second approach since THF is a liquid compound (sample labeled PPAC + THF).

Table 1 shows the concentrations used for each sample. These values were chosen following the concentrations used before by others in the literature for bulk hydrates [20, 28].

**Table 1.** Different additives used in the present study and their concentration in the mechanochemical and pre-impregnated systems.

			
Additives	Sodium dodecyl sulfate	Leucine	Tetrahydrofuran

Samples	[Additive] anchored to the PPAC	Samples	[Additive] in the solution (per g of water)
PPAC	----	PPAC	----
PPAC@SDS	0.3 g/g	PPAC + SDS	0.15 wt. %
PPAC@Leucine	0.2 g/g	PPAC + Leucine	0.1 wt. %
		PPAC + THF	5.56 mol%

Textural properties of the synthesized samples were evaluated by gas physisorption of nitrogen at  $-196^\circ\text{C}$ . Gas adsorption measurements were performed in a homemade fully automated manometric equipment designed and constructed by the Advanced Materials Group (LMA), now commercialized as N2GSorb-6 (Gas to Materials Technologies; [www.g2mtech.com](http://www.g2mtech.com)). The sample (*ca.* 100 mg) was previously degassed for 4 h at  $250^\circ\text{C}$  under vacuum ( $10^{-3}$  Pa). Nitrogen adsorption data were used to determine: (i) the total pore volume ( $V_t$ ) at a relative pressure of 0.95, (ii) the BET-specific surface area ( $S_{\text{BET}}$ ) and (iii) the

micropore volume ( $V_{N_2}$ ) by application of Dubinin–Radushkevich equation. The difference between  $V_t$  and  $V_{N_2}$  was used to calculate the mesopores volume ( $V_{meso}$ ).

Thermogravimetric experiments were carried out in a Mettler Toledo TGA/SDTA, located in the Research Technical Services of the University of Alicante (SSTTI). An alumina crucible containing 10 mg of sample was heated under  $100 \text{ ml}\cdot\text{min}^{-1}$  of  $N_2$  flow up to  $1000 \text{ }^\circ\text{C}$ , at a heating rate of  $10 \text{ }^\circ\text{C}\cdot\text{min}^{-1}$ .

XPS spectra were collected using a Thermo Scientific K-ALPHA with Al-K radiation ( $1486.6 \text{ eV}$ ), monochromatized by a twin crystal monochromator, yielding a focused X-ray spot with a diameter of  $400 \text{ }\mu\text{m}$ , at  $3 \text{ mA} \times 12 \text{ kV}$  when charge compensation was achieved with the system flood gun that provides low energy electrons and low energy argon ions from a single source. The alpha hemispherical analyzer was operated in the constant energy mode with survey scan pass energies of  $200 \text{ eV}$  to measure the whole energy band and  $50 \text{ eV}$  in a narrow scan to selectively measure the particular elements. The samples were further characterized by elemental analysis, with a Thermo Finnigan Flash 1112 Series with a Microelemental Analyser.

To grow the hydrate structures, the nanoporous carbon PPAC and the modified carbons (PPAC@Leucine and PPAC@SDS) were pre-humidified under water-supplying conditions denoted by  $R_w$  ( $R_w$ , represents the mass of water per mass of dry carbon). The  $R_w$  value selected is 4.1, that corresponds to the oversaturated sample (saturation capacity measured using water adsorption at  $25^\circ\text{C}$  is  $2.4 \text{ g}_{H_2O}/\text{g}_{AC}$ ). The same  $R_w$  conditions were applied for both approaches. To this end, water droplets (or water solution containing the additives) were added slowly with a syringe to the carbon grains, with manual agitation, up to the defined  $R_w$  value. High-pressure  $CH_4$  adsorption/desorption isotherms were measured at  $2^\circ\text{C}$  and  $-10^\circ\text{C}$  and up to  $10 \text{ MPa}$  in a homemade fully automated manometric equipment. Pre-humidified samples were frozen at  $-20 \text{ }^\circ\text{C}$  before the outgassing treatment to avoid any water loss.

Synchrotron X-ray powder diffraction data (SXRPD) were collected on the powder diffraction endstation of the MSPD beamline at synchrotron ALBA in Spain, using a MYTHEN detector and a wavelength of  $0.4129 \text{ \AA}$ . The experiments were performed in an ad hoc capillary reaction cell (fused silica capillary, inner diameter  $0.7 \text{ mm}$ , outer diameter  $0.85 \text{ mm}$ ). Thermal oscillations were described using overall Debye-Waller factor. Before the experiment the water pre-adsorbed carbon samples were placed inside the cell, which was connected via a capillary line to a gas-handling and a vacuum line. An Oxford Cryostream 700 was used to control the temperature of the sample.

### 3. Results and discussion

#### 3.1. Characterization of the mechanochemically modified carbons

Figure 1 shows the N<sub>2</sub> adsorption/desorption isotherms at -196°C for the PPAC sample before and after the mechanochemical modification with the different additives. As it can be appreciated, unmodified activated carbon exhibits a widely developed micro- and mesoporous structure with a total pore volume slightly below 3 cm<sup>3</sup>/g and a BET surface area above 3600 m<sup>2</sup>/g. These exceptional textural properties are associated with the optimum performance of KOH as a chemical activating agent to create a widely developed porous network. The presence of mesoporosity is also reflected in the desorption branch with a small hysteresis loop at  $p/p_0 = 0.5$ .

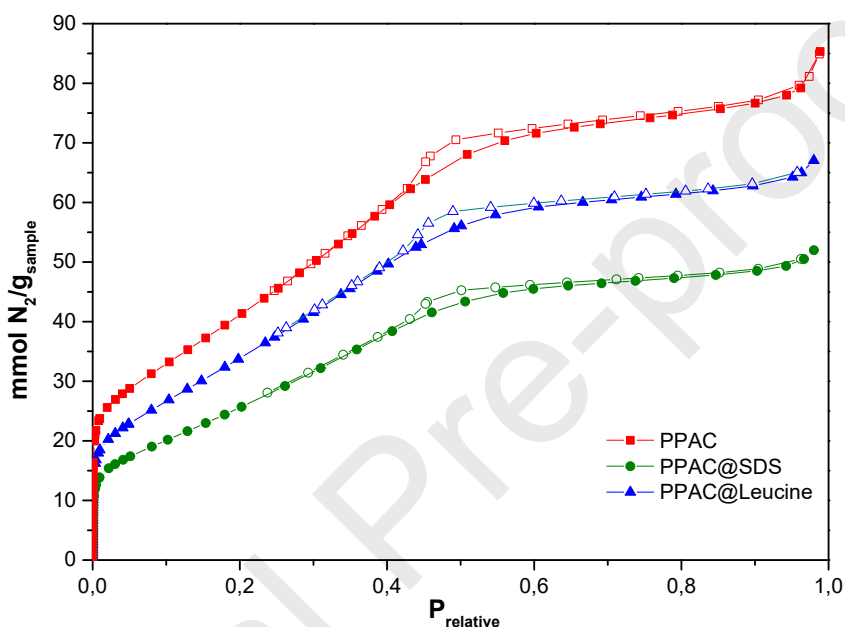


**Figure 1.** N<sub>2</sub> adsorption (full symbols)/desorption (open symbols) isotherms at -196°C for the evaluated samples

The samples modified through the mechanochemical approach with additives exhibit a significant reduction in the N<sub>2</sub> adsorption performance, thus reflecting the successful incorporation of the additive into the carbon structure. As shown in Table 2, the BET surface area decreases 22% and 36% after incorporation of Leucine and SDS, respectively, compared to the value for the unmodified activated carbon (even though this sample was also submitted to the ball-milling, but without additives). The larger decrease observed for the SDS-modified sample is in close agreement with the larger molecular size of this additive compared to leucine.

A closer look to the nitrogen adsorption isotherms suggests that the incorporation of the additives does not affect the shape of the isotherm but rather the total adsorption capacity, with a clear downshift over the whole relative pressure range evaluated. This observation reflects a preferential blocking of the



microporosity after the anchoring of the additive, as confirmed in Table 2. Most probably, the additives are anchored to the defects at the micropore entrance, thus explaining the preferential blocking of these pores, while mesopores remain less affected (above  $p/p_0 = 0.4$ , all isotherms are rather similar).

**Table 2.** Textural properties of the evaluated samples obtained from the  $N_2$  adsorption data at  $-196^\circ\text{C}$ .

sample	$S_{\text{BET}}$ ( $\text{m}^2/\text{g}$ )	$V_{\text{total}}$ ( $\text{cm}^3/\text{g}$ )	$V_{\text{micro}}$ ( $\text{cm}^3/\text{g}$ )	$V_{\text{meso}}$ ( $\text{cm}^3/\text{g}$ )	%V micro	%V meso	% micro lost	% meso lost
PPAC	3690	2.44	1.20	1.24	51	49	-	-
PPAC@Leucine	2860	2.00	0.80	1.20	40	60	33	4
PPAC@SDS	2350	1.75	0.65	1.10	37	63	46	12

The preferential blocking of the microporosity can also be appreciated in the pore size distribution (PSD) profiles described in Figure 2. QSDFT model describes a bimodal PSD, with a sharp contribution in the microporous range (around 1 nm) and a broad contribution in the wide microporous/small mesoporous region, with a maximum at around 3 nm. The preferential blocking of the micropores versus mesopores is evident from the PSD profiles after the anchoring of the additives.

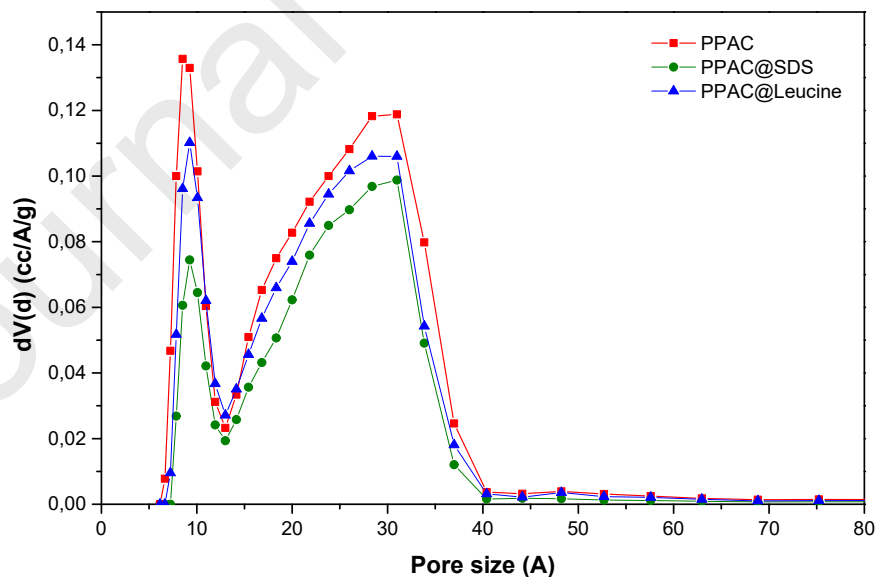


**Figure 2.** Pore size distribution obtained after application of the QSDFT method to the  $N_2$  adsorption data at  $-196^\circ\text{C}$  (slit-shaped; equilibrium model on carbon materials).

Although the presence of a significant structural blocking, even after an extensive washing step, can be considered *a priori* as a proof of the success of the mechanochemical approach, these samples have been further characterized using thermogravimetric measurements (TG), elemental analysis and X-ray photoelectron spectroscopy (XPS).

Figure 3a and 3b show the thermogravimetric analysis under  $N_2$  for (a) the pure compounds and (b) the activated carbons modified with the additives. In the specific case of the PPAC activated carbon, the TG profile is rather flat with a large thermal stability under inert atmosphere up to  $800^\circ\text{C}$ . This result is in close agreement with the thermal fingerprint of these kind of samples submitted to a high temperature thermal activation treatment ( $800^\circ\text{C}$  for 2h). Concerning the additives, the TG profiles show a similar performance for both organic molecules, their decomposition starting at around  $200\text{-}230^\circ\text{C}$  and reaching a plateau at around  $300^\circ\text{C}$ . Whereas the decomposition of leucine at  $280^\circ\text{C}$  generates no residue, the decomposition of SDS at  $260^\circ\text{C}$  gives rise to a residual mass of  $\sim 27\%$  attributed to  $\text{Na}_2\text{S}$ .

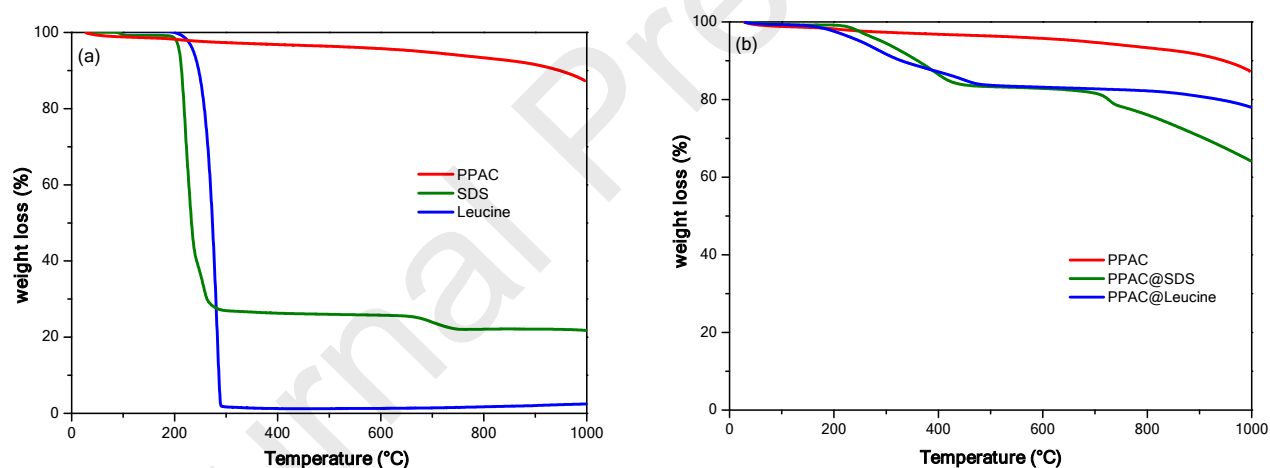


**Figure 3.** Thermogravimetric analysis under  $N_2$  flow for (a) pure compounds, and (b) PPAC activated carbons modified with additives.

Regarding the TG analysis of the modified carbon materials (Figure 3b), clear differences can be appreciated compared to the original PPAC sample. In the mechanochemically modified samples the decomposition of the additives starts at slightly higher temperatures,  $250\text{-}300^\circ\text{C}$ , but contrary to pure compounds, here the mass loss is more gradual and remains until  $425^\circ\text{C}$ . Apparently, the confinement

effects in carbon materials improve the stability of the anchored species. Interestingly, the performance is rather similar for both additives, the overall mass loss at 600°C being approximately 20% for both samples. For the specific case of the carbon modified with SDS, considering that 1 g of sample contains 0.3 g of Leucine (30 wt.%), and that pure SDS losses only 70% (Figure 3a) of its initial weight, the theoretical weight loss will be 21%, in close agreement with the observations. In the specific case of the leucine, the 20 wt.% loss perfectly agrees with the theoretical amount incorporated, assuming complete decomposition of leucine below 600°C (Figure 3a).

Table 3 shows the elemental analysis of the different activated carbons evaluated, including the analysis of the additives. All values have been compared with the theoretical ones.

**Table 3.** Elemental analysis composition (wt.%) of evaluated samples and pure components. (\*)  
Theoretical values are deduced from the chemical formula.

SAMPLE	Nitrogen (%)	Carbon (%)	Hydrogen (%)	Sulphur (%)	Oxygen (%)
SDS <sub>theoretical</sub> *	0.00	50.00	8.68	11.11	22.22
SDS	0.00	50.45	8.88	0.00	40.67
Leucine <sub>theoretical</sub> *	10.70	55.00	9.92	0.00	24.43
Leucine	10.80	55.76	10.43	0.00	23.00
PPAC	0.04	94.84	0.00	0.00	5.12
PPAC@SDS	0.00	84.35	1.85	0.00	13.80
PPAC@Leucine	3.44	85.26	7.21	0.00	4.09

As it can be appreciated, experimental and theoretical values for the pure additives are practically identical, with the exception of the oxygen and sulphur elements. It is well known that elemental analysis is especially useful for the determination and quantification of elements such as nitrogen, carbon, hydrogen. However, the amount of oxygen present in the samples is obtained as the difference with respect to the rest of elements, with the associated uncertainty in the quantification. In the same way, it is well-known that the quantification of sulphur is also quite difficult through elemental analysis, thus explaining the divergencies observed for these two elements.

Regarding the original activated carbon, it shows a very rich carbon content (around 95%), with very little content of heteroatoms, mainly oxygen due to the pyrolysis step and the subsequent activation at 800°C.

The incorporation of SDS decreases the carbon content, while the amount of oxygen and hydrogen increases. A similar situation takes place after incorporation of leucine with the detection of nitrogen and hydrogen from the organic additive. These numbers confirm the presence of the additive in the inner porous structure, with a rather similar percentage to the nominal values (Table 3; assuming an additive loading of 20 wt.% and 30 wt.%, for PPAC@Leucine and PPAC@SDS, respectively, theoretical amount of nitrogen and sulphur must be around 2-3 wt.%).

To further analyze the chemical composition of the modified carbons, the three samples have been evaluated using X-ray photoelectron spectroscopy (XPS). Since XPS is a surface-sensitive technique, it can be very useful to estimate the dispersion of the additives in the carbon structure by comparison with elemental analysis. Table 4 shows the surface composition for the evaluated samples. As expected, the original carbon material (PPAC) exhibits a rich carbon content (> 97%), in close agreement with elemental analysis. The successful incorporation of the additives is confirmed by the decrease in the carbon content and the associated detection of sodium and sulphur (for PPAC@SDS), and nitrogen and oxygen (for PPAC@Leucine). In summary, these results confirm the presence of additives in the carbon structure homogeneously distributed (in the surface and in the bulk), most probably anchored to the carbon structure.

**Table 4.** Surface composition of evaluated samples obtained from XPS.

Sample	ATOMIC RATIO %				
	Carbon	Oxygen	Sodium	Sulphur	Nitrogen
PPAC	97.22	2.73	-	0.05	-
PPAC@SDS	90.45	6.53	1.38	1.64	-
PPAC@Leucine	95.69	3.41	-	-	0.9

### 3.2. High-pressure methane adsorption isotherms for the mechanochemically modified carbons

The methane adsorption performance of the synthesized activated carbons has been evaluated up to 10 MPa and at two different temperatures, i.e. 2°C and -10°C. As it can be observed in Figure 4, the unmodified PPAC sample exhibits a Langmuir type isotherm with a final excess amount adsorbed as large as 25 wt.% ( $0.25 \text{ g}_{\text{CH}_4}/\text{g}_{\text{AC}}$ ) and 29 wt.% ( $0.29 \text{ g}_{\text{CH}_4}/\text{g}_{\text{AC}}$ ), respectively, for the two temperatures evaluated. These values are in close agreement with previous studies described in the literature and constitute among the best values described so far for high-pressure methane storage [29]. At low pressures preferentially micropores participate in the adsorption process, whereas at high-pressure also mesopores

exhibit a dominant role. It is important to highlight that the methane adsorption isotherms are fully reversible over the whole pressure range evaluated. The incorporation of the additives into the carbon skeleton gives rise to a decrease in the methane storage capacity over the whole pressure range evaluated, in close agreement with nitrogen adsorption measurements described above. The amount adsorbed decreases down to 23 wt.% and 19 wt.% at  $-10^{\circ}\text{C}$  for PPAC@Leucine and PPAC@SDS, respectively. A similar behavior is reflected at  $2^{\circ}\text{C}$ , the total amount adsorbed decreasing down to 18 wt.% and 15 wt.% upon functionalization. A closer look to the isotherms clearly shows that the reduction in the methane storage capacity is more significant at low pressures, below 5 MPa, due to the preferential blocking of the microporosity and narrow mesoporosity, as anticipated above.

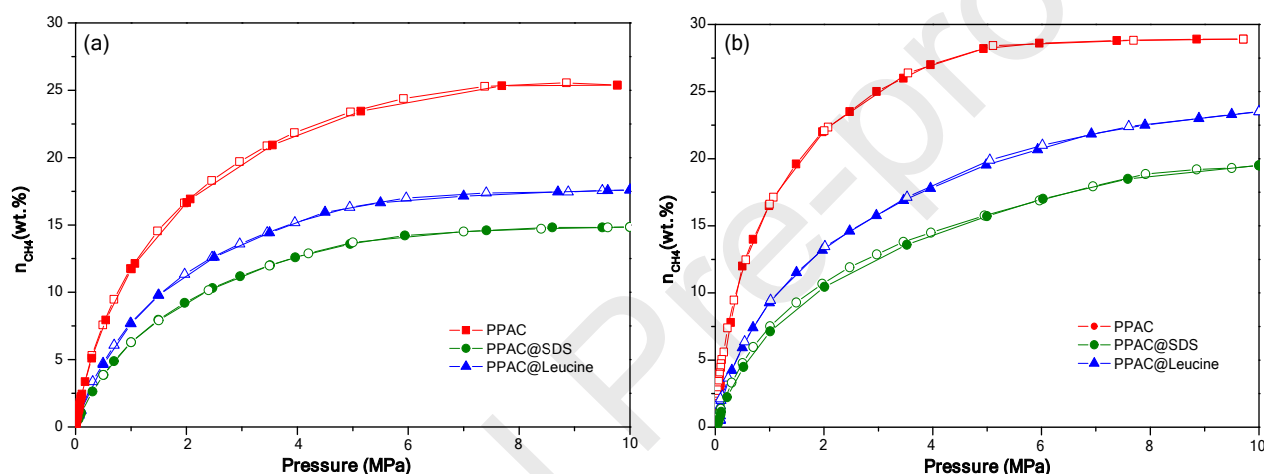


**Figure 4.**  $\text{CH}_4$  adsorption/desorption isotherms ( $\text{g}_{\text{CH}_4}/100\text{g}_{\text{carbon}}$ ) for the evaluated samples under dry conditions at (a)  $2^{\circ}\text{C}$  and (b)  $-10^{\circ}\text{C}$ .

To further analyze the adsorption performance, the packing density for methane (grams of methane adsorbed per pore volume ( $\text{cm}^3$ )) was estimated assuming that the methane is adsorbed only in micropores or in the whole porosity (micro-/mesopores). It has been widely reported in the literature that the packing density of methane in activated carbon materials oscillate between  $0.15\text{-}0.25\text{ g/cm}^3$ , depending on the kind of carbon and the pore size/shape [3, 7, 30]. The packing density for methane adsorbed at 10 MPa, assuming that only micropores participate in the adsorption process, takes values as high as  $0.20\text{-}0.23\text{ g/cm}^3$ , in close agreement with the literature (Table 5). Only when the total porosity is considered ( $V_{\text{total}}$ ), the packing density decreases down to  $0.09\text{ g/cm}^3$ , thus reflecting that mainly

micropores and most probably narrow mesopores participate in the adsorption process rather than the whole porous network.

**Table 5.** Excess methane adsorption capacity at 2°C and -10°C in the original activated carbon and the carbon modified with additives. Packing density considering that methane is adsorbed only in micropores or considering it is adsorbed in the whole porosity.

sample	CH <sub>4</sub> adsorption (g/g)		CH <sub>4</sub> packing density at 2°C (g/cm <sup>3</sup> )	
	T= 2°C	T=-10°C	Considering adsorption in total pore volume	Considering adsorption only in micropores
<b>PPAC</b>	0.24	0.28	0.098	0.20
<b>PPAC@SDS</b>	0.15	0.19	0.085	0.23
<b>PPAC@leucine</b>	0.18	0.23	0.088	0.22

After measuring the physisorption isotherms under dry conditions, samples were pre-humidified with water up to  $R_w = 4.1$  and further evaluated in the high-pressure adsorption process with methane. In a first approach, only the unmodified sample was evaluated up to 10 MPa (original PPAC pre-loaded with  $4.1 \text{ g}_{\text{H}_2\text{O}}/\text{g}_{\text{AC}}$ ) and compared with the bulk system (maintaining the same amount of water used in the pre-impregnation but spread in the reactor without the carbon). Figure 5 shows the high-pressure isotherms for both systems (referred as  $\text{g}_{\text{CH}_4}$  adsorbed per  $\text{g}_{\text{H}_2\text{O}}$  incorporated). The bulk system exhibits a rather flat adsorption profile, thus reflecting the absence of methane hydrate formation up to 10 MPa. This observation is in close agreement with previous bulk phase experiments and reflects the slow nucleation and growth kinetics in the bulk system [31, 32]. Only an amplification of the isotherm allows to appreciate a small jump at 4.5 MPa due to the formation of some isolated hydrate crystals at the gas-liquid interphase. During the desorption, the dissociation of the methane hydrate is slightly shifted to lower pressure, i.e. at 3.5 MPa, with the associated hysteresis loop. This hysteresis loop demonstrates that the methane hydrate formation process is defined by kinetics rather than thermodynamics [31-33]. The dissociation value perfectly fits to the P-T thermodynamic diagram of clathrates in nature, whereas the formation pressure is shifted to higher values [12]. When the same amount of water is spread in the carbon sample, the high-pressure adsorption isotherm changes drastically. Below 3.5 MPa the isotherm is completely flat, thus confirming the complete blocking of the porosity by pre-adsorbed water. However,

above this threshold pressure, the amount of methane adsorbed exhibits a drastic increase up to 5.0 MPa, followed by a small plateau. Above 7.0 MPa, the amount of methane adsorbed further increases up to a maximum of  $0.16 \text{ g}_{\text{CH}_4}/\text{g}_{\text{H}_2\text{O}}$  at 10 MPa (vs  $0.012 \text{ g}_{\text{CH}_4}/\text{g}_{\text{H}_2\text{O}}$  in the bulk system). These results constitute a 12-fold increase in the water-to-hydrate conversion yield promoted by the confinements effects in the activated carbon. Interestingly, the confined hydrates are highly stable down to 3.0 MPa, the dissociation being extremely drastic afterwards. Based on the thermodynamics of gas hydrates, the first adsorption step between 3.5 MPa and 7.0 MPa must be attributed to methane hydrate formation in the external surface area and large cavities, whereas the second step above 7.0 MPa must be attributed to the nucleation and growth in narrower cavities (mainly micro- and mesopores) [34].

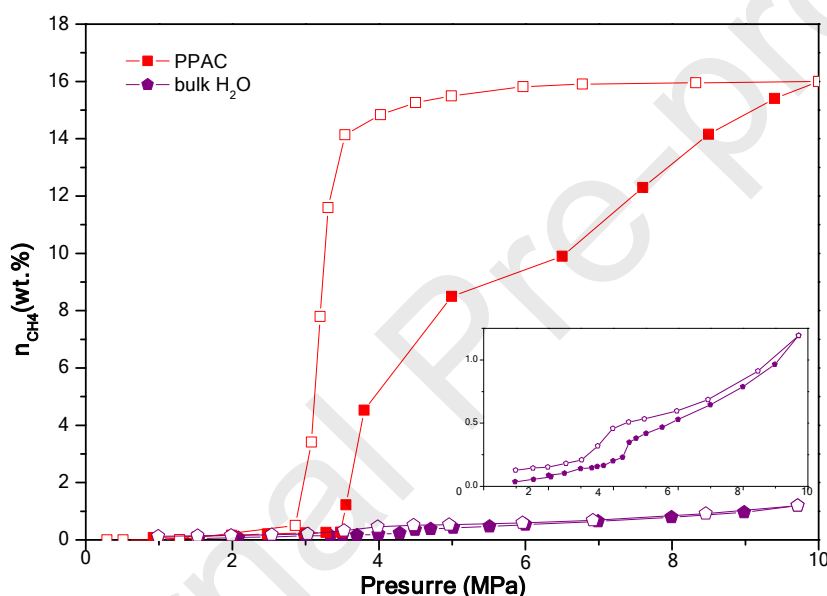


**Figure 5.** High-pressure  $\text{CH}_4$  adsorption (closed symbols)/desorption (open symbols) isotherms ( $\text{g}_{\text{CH}_4}/100\text{g}_{\text{H}_2\text{O}}$ ) at  $2^\circ\text{C}$  for the pre-impregnated PPAC activated carbon ( $R_w:4.1$ ) and bulk water (see inset for a larger resolution).

From the amount of  $\text{CH}_4$  stored at 10 MPa and the amount of water incorporated in the pre-adsorption step, hydrate stoichiometries could be estimated. In the specific case of bulk water, the calculated stoichiometry is  $1 \text{ CH}_4:74\text{H}_2\text{O}$ , quite far from the stoichiometry in natural hydrates ( $1 \text{ CH}_4:5.75 \text{ H}_2\text{O}$ ). This result clearly reflects that the water-to-hydrate yield is extremely small (around 8%) under bulk conditions. However, in the water-confined carbon system the calculated stoichiometry is  $1 \text{ CH}_4:5.5 \text{ H}_2\text{O}$ ,

thus confirming a conversion >95%, in close agreement with previous differential calorimetry analysis [35].

Figure 6 describes the methane hydrate formation process in the PPAC carbon sample after the mechanochemical modification with additives. Although the amount of water incorporated in these samples remains constant ( $R_w = 4.1$ ), the adsorption performance is rather different. At this point it is important to highlight that these experiments were performed only at  $-10^\circ\text{C}$  to identify differences in the PPAC sample with the adsorption temperature. At  $-10^\circ\text{C}$  the shape of the isotherm for un-modified PPAC is rather similar to  $2^\circ\text{C}$ , although important differences are observed in the pressure thresholds. Under these conditions, the blocking effect exerted by pre-adsorbed water prevails only up to 1.7 MPa, the amount adsorbed drastically changing afterwards. Under these conditions, the driving force required to enhance the nucleation process is lower. In the same way, the second nucleation step (inside micro- and mesopores) is also shifted to lower pressures (*ca.* 3.5 MPa). This observation denotes an important effect of the adsorption temperature in the thermodynamics of the methane hydrate nucleation process [12]. In any case, the total amount adsorbed at 10 MPa is as high as 82 wt.% (or 0.82 g  $\text{CH}_4$  per g of dry carbon). Compared to the dry PPAC carbon (29 wt.%), this result constitutes an extraordinary increase in the methane storage capacity through the so-called solid storage approach.

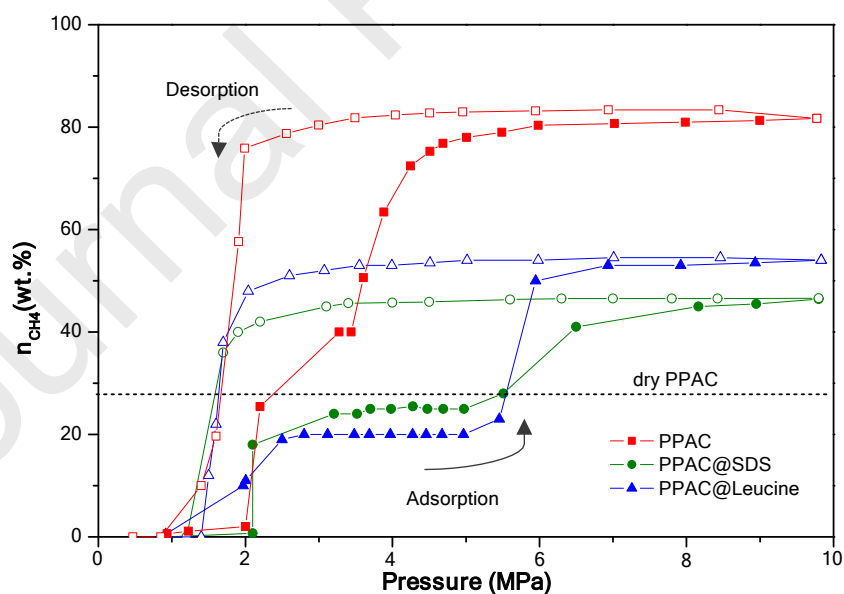


**Figure 6.**  $\text{CH}_4$  adsorption (closed symbols)/desorption (open symbols) isotherms (wt.% or  $\text{g}_{\text{CH}_4}/100\text{g}_{\text{carbon}}$ ) at  $-10^\circ\text{C}$  for PPAC and PPAC-modified carbons under wet conditions ( $R_w=4.1$ ).



Incorporation of additives in the PPAC carbon material gives rise to important differences. Below 2.5 MPa, the three isotherms are rather similar thus reflecting that the first nucleation step, i.e. the one taking place in the external surface and in wide pores, may not be affected *a priori* by the incorporation of additives. This observation agrees with the preferential location of the additives in the inner porous network, as suggested by N<sub>2</sub> adsorption data. However, above 3 MPa, samples modified with additives (PPAC@Leucine and PPAC@SDS) exhibit a marked plateau that remains stable up to 5.5 MPa, for Leucine, and 6.0 MPa, for SDS. Apparently, the presence of additives inhibits the second nucleation process to high pressures. Considering that the second step corresponds to nucleation processes taking place in the inner pores of the carbon network, the inhibition observed constitutes another proof about the successful incorporation of the additives in the inner porosity. Above 5.5-6.0 MPa both samples exhibit a second jump in the adsorption isotherm, although the amount of methane adsorbed in this second process is much lower compared to the unmodified PPAC carbon (in the absence of additives). The total amount stored in the modified PPAC samples reach values around 55 wt.% and 46 wt.% for Leucine and SDS-based samples, respectively. Interestingly, all these changes in the methane hydrate nucleation process are not reflected in the dissociation step since, in all cases, confined hydrates dissociate at 1.7 MPa. Consequently, the incorporated additives inhibit the methane hydrate nucleation process in the narrower pores, maybe due to steric/kinetic restrictions, whereas dissociation follows thermodynamics. Most probably, the anchored organic moieties act as steric modifiers altering the normal crystal growth. The similar performance for both additives, independently of their characteristics, reinforce this hypothesis. Last but not least, it is important to highlight that despite having the same amount of water pre-adsorbed, the total uptake at 10 MPa is reduced after the incorporation of the additives.

In summary, these results confirm that the presence of additives anchored to the carbon surface does not exhibit any promoting effect in the methane hydrate formation process. The presence of additives limits the total uptake, due to steric effects, and inhibits the nucleation process in the inner pores with a shift to higher pressures compared to the unmodified carbon. The relatively low-pressure threshold for hydrate formation, and the large methane uptake at 10 MPa confirms PPAC as the best nanoporous adsorbent described till date for methane hydrate formation.

### *3.3. High-pressure methane adsorption isotherms for the additive's pre-impregnated carbons*

As a last step of this study, the effect of the additives has been evaluated when dissolved in ultrapure water, before the pre-loading of the PPAC sample. As described in the experimental section, THF is also included in this section as a potential additive to modify the thermodynamics and kinetics of these

nucleation processes. THF is a liquid and it has been proposed as a promotor for hydrate formation. THF promotes the sII hydrate structure by occupying the larger cavities, whereas unmodified hydrates crystallize in the sI structure [21, 22]. Figure 7 shows the high-pressure  $\text{CH}_4$  isotherms at  $2^\circ\text{C}$  for the PPAC activated carbon pre-impregnated with pure water or water modified with additives (at  $R_w = 4.1$ ).

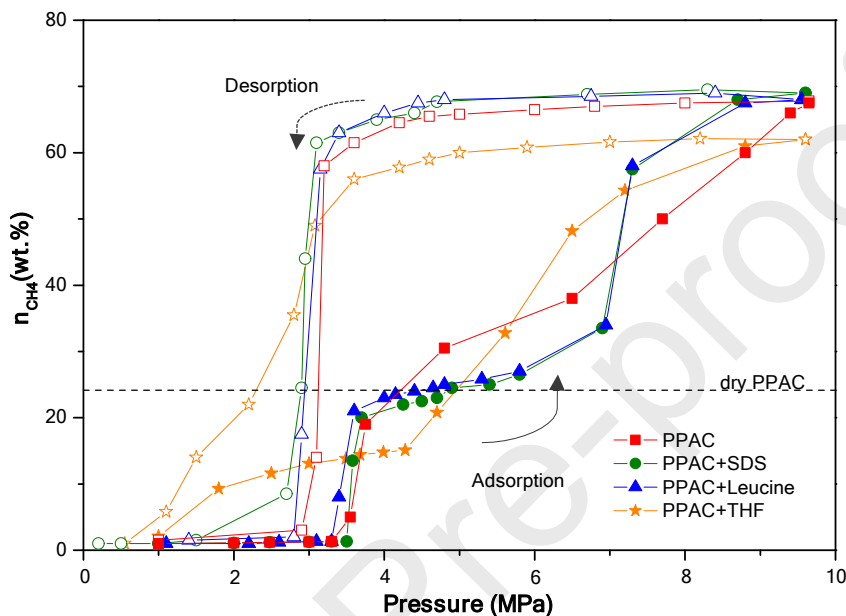


**Figure 7.**  $\text{CH}_4$  adsorption (closed symbols)/desorption (empty symbols) isotherms (wt.% or  $\text{g}_{\text{CH}_4}/100\text{g}_{\text{carbon}}$ ) at  $2^\circ\text{C}$  for sample PPAC impregnated with water and water dissolved additives.

As it can be appreciated in Figure 7, at low pressures samples PPAC, PPAC+Leucine and PPAC+SDS perform quite similar with a complete inhibition in the adsorption uptake up to 3.5 MPa. This value corresponds to the pressure threshold usually observed for natural hydrates at  $2^\circ\text{C}$ . After a sharp increase in the methane uptake, samples PPAC+Leucine and PPAC+SDS exhibit an important plateau (at 25 wt.%) due to the inhibition of the second nucleation process, in close agreement with previous results for the surface-modified samples. However, once the pressure reaches 6.0-7.0 MPa, both samples exhibit a sudden increase, the final uptake being rather similar to the pure-water PPAC system (*ca.* 69 wt.% or 0.69  $\text{g}_{\text{CH}_4}/\text{g}_{\text{carbon}}$ ). These results confirm that both additives exhibit a similar promoting effect, independently of their nature.

The scenario is completely different with THF. For this specific additive, the methane hydrate formation already starts at around 1.2-1.5 MPa, quite below the thermodynamic threshold pressure, with a plateau

at 15 wt.%. At 4.2 MPa the adsorption isotherm exhibits a second increase up to a total uptake at 10 MPa around 62 wt.%. These results clearly show that even under confinement conditions, THF is a thermodynamic promoter. Both nucleation processes, in the external surface and in the inner pores of the carbon, are promoted at much lower pressures compared to the confined pure-water system. Concerning the differences in the final methane uptake (ca. 7 wt.% lower in the presence of THF), these differences comes preferentially from the first nucleation step. As shown later, hydrate crystals grown in the external surface and large pores under THF conditions exhibit a sII structure with shared occupation of small ( $\theta_{sc}$ ) and large ( $\theta_{lc}$ ) cages between  $\text{CH}_4$  and THF, thus explaining the limited amount of methane stored. On the contrary, methane hydrates grown in the inner pores (second step) resemble those on the pure water-based PPAC sample. In any case, a significant hysteresis loop can be appreciated due to the improved stability of confined hydrates towards dissociation in the presence of THF.

The knowledge of the amount of methane adsorbed, from the high-pressure isotherm, and the knowledge of the amount of water pre-adsorbed, from the sample preparation, allows to estimate, quantitatively, the stoichiometry of the synthesized hydrates.

**Table 6.** Stoichiometry of the methane hydrates synthesized in the absence and presence of additives considering the amount of water incorporated and the methane consumption. The stoichiometry has also been calculated assuming the total amount adsorbed and assuming the two steps at mid- and high-pressure.

Sample	Total	Stoichiometry	Stoichiometry
	stoichiometry	1st step	2nd step
PPAC	1 $\text{CH}_4 \cdot 5.3 \text{H}_2\text{O}$	1 $\text{CH}_4 \cdot 6.0 \text{H}_2\text{O}$	1 $\text{CH}_4 \cdot 4.8 \text{H}_2\text{O}$
PPAC + Leucine	1 $\text{CH}_4 \cdot 5.4 \text{H}_2\text{O}$	1 $\text{CH}_4 \cdot 6.3 \text{H}_2\text{O}$	1 $\text{CH}_4 \cdot 4.7 \text{H}_2\text{O}$
PPAC + SDS	1 $\text{CH}_4 \cdot 5.4 \text{H}_2\text{O}$	1 $\text{CH}_4 \cdot 6.3 \text{H}_2\text{O}$	1 $\text{CH}_4 \cdot 4.7 \text{H}_2\text{O}$
PPAC + THF	1 $\text{CH}_4 \cdot 5.9 \text{H}_2\text{O}$	1 $\text{CH}_4 \cdot 8.9 \text{H}_2\text{O}$	1 $\text{CH}_4 \cdot 4.5 \text{H}_2\text{O}$

As it can be observed, the total stoichiometry at 10 MPa is in close agreement with natural and bulk methane hydrates, i.e. 1  $\text{CH}_4 \cdot 5.7 \text{H}_2\text{O}$ , attributed to the structure sI. In particular, for samples PPAC, PPAC+Leucine and PPAC+SDS, the obtained values are slightly lower than theoretical, around 1  $\text{CH}_4 \cdot 5.3 \text{H}_2\text{O}$ . The under-stoichiometric behavior can be attributed to i) the formation of non-stoichiometric hydrates in narrow cavities or ii) to the presence of free-adsorbed methane in narrow cavities, non-forming hydrates [24]. On the contrary, for the specific case of the THF-based sample, the obtained value

is slight above the theoretical prediction, i.e. there is a certain excess of water ( $1 \text{ CH}_4 \cdot 5.9 \text{ H}_2\text{O}$ ), due to the participation of THF in the hydrate structure.

Considering the amount of methane adsorbed in the two steps of the high-pressure isotherms, and assuming that the first step corresponds to water pre-adsorbed in large pores ( $1.7 \text{ g}_{\text{H}_2\text{O}}/\text{g}_{\text{AC}}$ , except for THF-based sample where  $1.5 \text{ g}_{\text{H}_2\text{O}}/\text{g}_{\text{AC}}$  was adsorbed) and the second step corresponds to water in the inner pores (saturation at  $2.4 \text{ g}_{\text{H}_2\text{O}}/\text{g}_{\text{AC}}$ ), the stoichiometry has been estimated in these two specific cases [24]. Although this is a rough estimation, it allows to gain more knowledge about the nature of the confined hydrates. As expected, the stoichiometry is much closer to the natural or bulk system in the first step, i.e. hydrates grown in the external surface resembles natural or bulk hydrates. On the contrary, under-stoichiometric conditions are obtained in the second step, due to the steric constrictions in narrow mesopores and micropores. Only THF-based hydrates do not follow this tendency, at least in the first step, with a stoichiometry of  $1 \text{ CH}_4 \cdot 8.9 \text{ H}_2\text{O}$ . The deficiency of methane in the first step anticipates a different nature of the hydrates formed under these conditions (maybe due to the presence of the sII structure).

Last but not least, the kinetics of the hydrate nucleation process at 3.6 MPa have been compared for pure water and water-modified with the different additives (except THF). Figure 8 compares the time (in hours) required for this specific pressure point (that corresponds to the initiation of the hydrate nucleation process) to reach equilibrium. The time required by this pressure point to reach equilibrium indirectly reflects the induction time required for the nucleation process to start in the external surface and/or in large cavities.

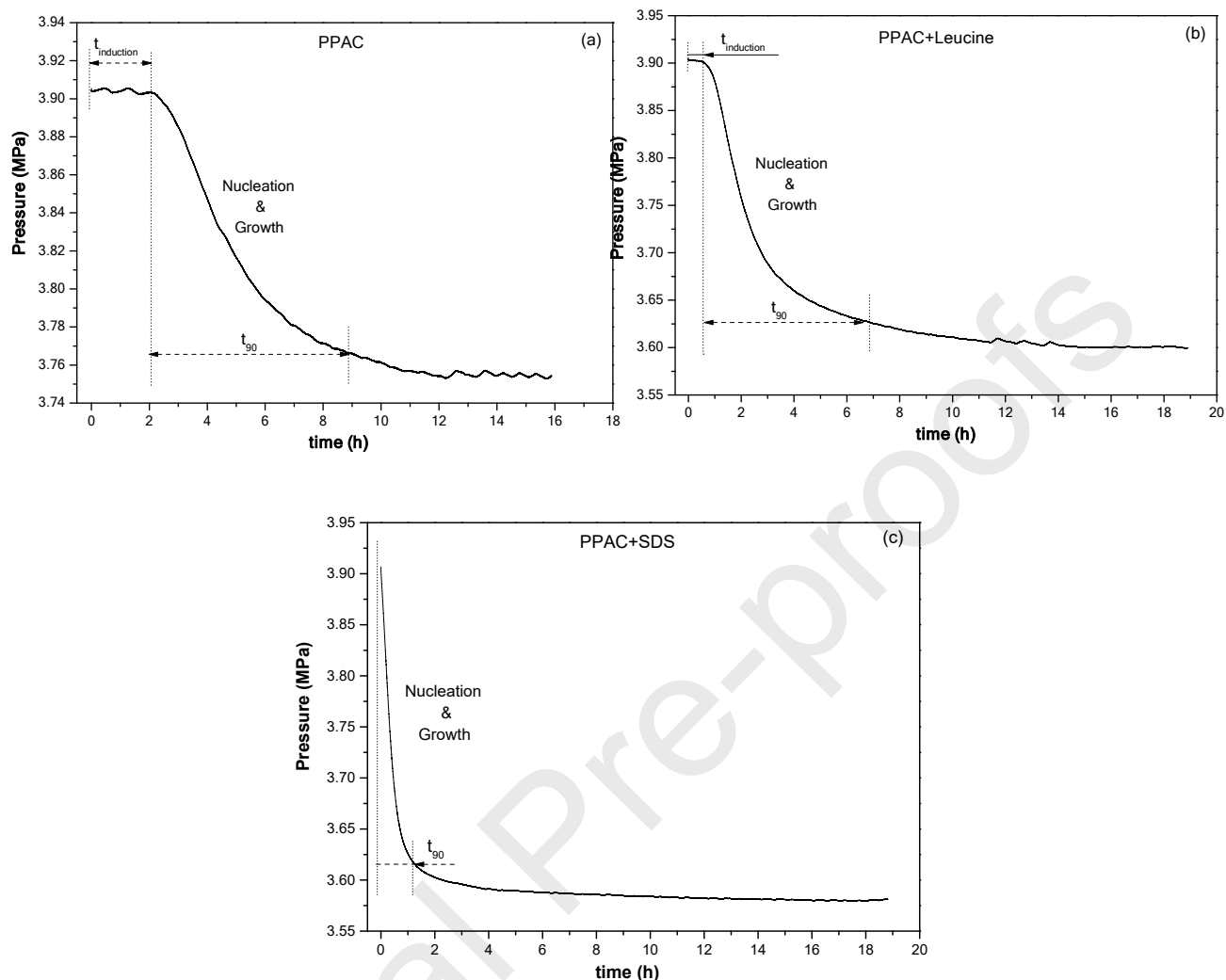


**Figure 8.** Gas consumption versus time at the manifold for a pressure of 3.6 MPa. Figures include the induction time (before nucleation) and the time required to reach 90% of the water-to-hydrate conversion at this specific pressure point.

As it can be appreciated in Figure 8, PPAC carbon pre-adsorbed with ultra-pure water exhibits an initial induction time of 2.1 h. After this induction period, the methane hydrate nucleation and growth start, 90% of the conversion ( $t_{90}$ ) been reached in 6.8h. For the sample pre-adsorbed with an aqueous solution of leucine, the induction time decreases to 0.4h, while 90% equilibrium is reached in 6h. Last but not least, in the presence of SDS, the induction time is completely suppressed and the  $t_{90}$  is reached in 1h. This observation constitutes a real prove about the beneficial role exerted by additives in the kinetics of the water-to-hydrate conversion process. The obtained result constitutes a tremendous improvement in the

kinetics compared to bulk water (under static conditions and without agitation, bulk water require weeks or months to convert water-to-hydrate, see Figure 5), thus explaining the beneficial role of carbon in these nucleation processes. SDS and Leucine have a solubility in water at 20°C of 150 mg/ml and 24 mg/ml, respectively, i.e. SDS has a solubility in water more than 6 times larger compared to leucine [36, 37]. Considering that the solubility of the surfactant also helps to increase water activity, this observation can explain the observed differences. Water activity could be define as the ability to form hydrated compounds [38]. When activity is low, less molecules are free, so hydrate formation is shifted towards higher pressure and temperature. Also, the decrease of water activity, for instance by using methanol, hinders the hydrate nucleation [39]. Similar studies from our research group have shown that the presence of a saline environment can also modify the water activity and the associated hydrate formation [25]. In the specific case of THF solution it is difficult to compare the induction time at 3.6 MPa, since the nucleation of gas hydrates already started at lower pressures (Figure 7).

#### *3.4. Synchrotron X-ray powder diffraction (SXRPD) analysis of the confined hydrates in the presence of THF*

Although *sl* is the traditional crystal structure observed for methane hydrates, either in bulk or confined in nanoporous carbon materials, it is well-known in the literature that the incorporation of THF can promote the *sII* structure [22]. The unit cell of the *sl* structure consists of two kinds of cavities: two pentagonal dodecahedra ( $5^{12}$ ) cavities (small cavities) and six tetrahedra ( $5^{12} 6^2$ ) (large cavities), and 46 water molecules. If each cavity host one methane molecule, the final stoichiometry is  $1 \text{ CH}_4 \cdot 5.75 \text{ H}_2\text{O}$ . In the case of the *sII* structure, there are also two kind of cavities: sixteen small distorted pentagonal dodecahedra ( $5^{12}$ ) and eight large hexadecahedra ( $5^{12} 6^4$ ), with 136 water molecules [12]. In this case, for complete occupancy, the nominal stoichiometry is  $1 \text{ CH}_4 \cdot 5.67 \text{ H}_2\text{O}$ .

In order to confirm the potential role of confinement in the promotion of the *sl* and/or *sII* structure before and after the addition of THF, samples PPAC and PPAC+THF have been evaluated using synchrotron X-ray powder diffraction (SXRPD) (Figure 9). The number of studies in the literature dealing with SXRPD evaluation of gas hydrates is scarce and, to our knowledge, none of these studies deals with confined hydrates.

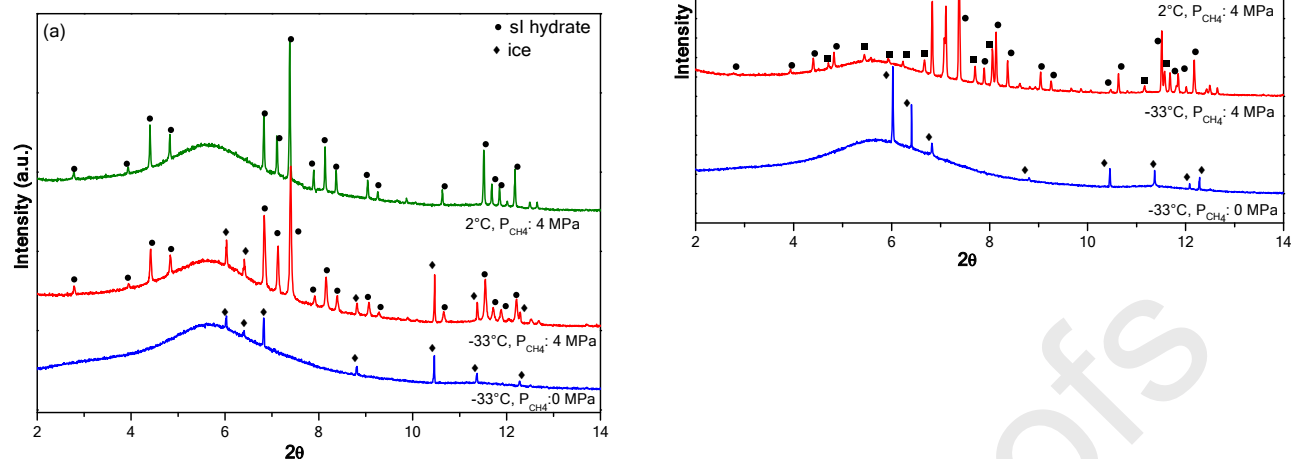


**Figure 9.** Synchrotron X-ray powder diffraction patterns (SXRPD) of PPAC sample (a) in the presence of pure water and (b) in the presence of water+THF. Bottom spectra corresponds to atmospheric pressure conditions and middle-upper spectra corresponds to pressurization with 4.0 MPa  $\text{CH}_4$ .

As it can be observed in Figure 9a, the PPAC sample impregnated with water at  $-33^\circ\text{C}$  gives rise to the characteristic peaks of a hexagonal ice structure ( $I_h$ ). After the system is pressurized with 4.0 MPa  $\text{CH}_4$ , the characteristic peaks of methane hydrate with a si structure can be clearly appreciated, although the conversion is not complete and some ice remains. Further heating up to  $2^\circ\text{C}$  is required for the complete conversion of the ice to the methane hydrate (although we cannot exclude the presence of some liquid water). When the same experiments are performed with sample PPAC pre-adsorbed with a water solution containing THF, the situation changes. The original pre-adsorbed sample at  $-33^\circ\text{C}$ , before pressurization, also shows the characteristic peaks of hexagonal ice, in close agreement with the pure water experiments. A subsequent pressurization with 4.0 MPa methane gives rise to a mixture of si and sII structure, the proportion of these two structures being rather similar even at the highest temperature evaluated ( $2^\circ\text{C}$ ). In order to obtain the quantitative characteristics of the selected samples, including cage occupancy for small and large cages ( $\theta_{sc}$  and  $\theta_{lc}$ ), the Rietveld refinement has been applied to fit the SXRPD patterns. The occupancies of the cages by guest molecules were fixed at 1 for the positions where the refinement did not give significant improvement of the fitting quality. Figure 10 shows the fitting results for the samples at  $2^\circ\text{C}$  and 4.0 MPa.

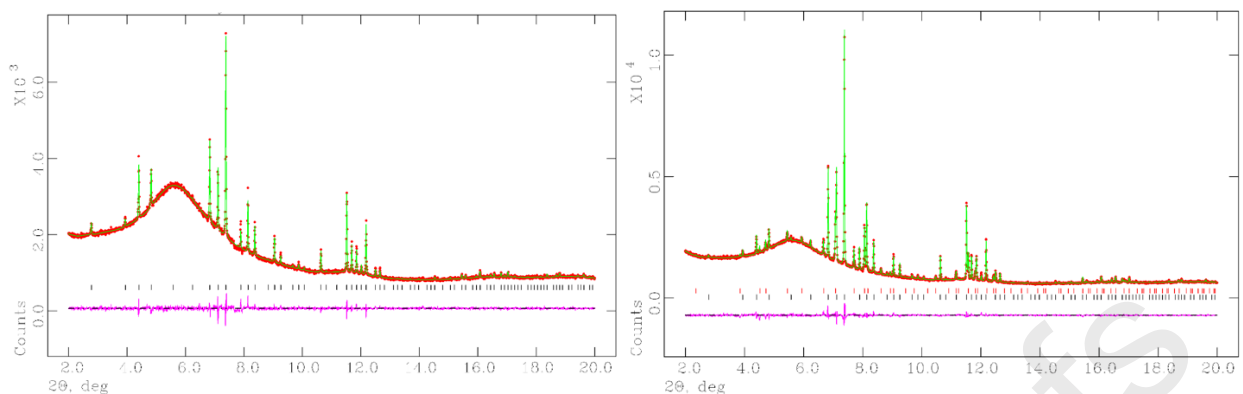


**Figure 10.** Rietveld refinement of the PPAC system (left panel) and PPAC+THF (right panel) at 2°C and 4.0 MPa of CH<sub>4</sub>.

**Table 7.** Structural parameters obtained for the confined methane hydrates in sample PPAC pre-adsorbed using pure water ( $P_{\text{CH}_4} = 4.0$  MPa).

Sample	Temperature, °C	sl phase				
		a, Å	$\theta_{\text{SC}} (5^{12})$	$\theta_{\text{LC}} (5^{12}6^2)$	wt %	size, nm
PPAC + H <sub>2</sub> O+ CH <sub>4</sub>	-33	11.9425(2)	methane 1 (not refined)	methane 0.82(1)	78.9 (21.1 ice)	81
PPAC + H <sub>2</sub> O+ CH <sub>4</sub>	2	11.9938(3)	methane 0.95(2)	methane 0.64(1)	100	215

The confined methane hydrates in sample PPAC exhibit a cubic structure with a  $Pm3n$  space group with cell parameters ranging from  $a = 11.9425(2)$  to  $11.9938(3)$  Å. These values are somewhat larger compared to those described in the literature for artificial bulk hydrates [40, 41]. The difference probably comes from the smaller size for confined crystals. The ice content at low temperatures (-33°C) derived from the refinement is around 21 wt.%, while the gas-to-hydrate conversion scales up to 100% at 2°C.

As it can be appreciated in Table 7, at low temperatures the small cages are fully occupied by methane molecules, whereas large cages occupation is 0.82. This result is surprising since previous studies with bulk methane hydrates and thermodynamic models anticipate a preferential occupation of large cages already at low pressure (around 100%), whereas small cages exhibit a cage occupancy of around 0.8-0.9 at the pressures used in our study [40, 42]. Most probably this unusual cavity filling is due to the confinement effects and the enhanced pressure in narrow pores. For a cage occupation of  $\theta_{\text{SC}} = 1$  and  $\theta_{\text{LC}} = 0.82$ , the predicted stoichiometry from the synchrotron XRD data is  $1 \text{ CH}_4 \cdot 6.6 \text{ H}_2\text{O}$ , in close agreement



with the value obtained from the high-pressure isotherms (Table 6). Last but not least, it is important to highlight a significant thermal expansion of the obtained methane hydrates [43], as well as a remarkable decrease of the occupancy of the large cages at 2°C. The last effect highlights relatively fast gas diffusion across the large cavities and suggests close to equilibrium filling of these positions.

Table 8 reports the structural parameters deduced after applying Rietveld refinement to the XRD data for the sample PPAC + THF. As described above, upon pressurization this sample exhibits a combination of sI and sII structures. The weight percentage of sI and sII structures in the two temperatures evaluated is ca. 75% for sI and ca. 25% for sII. Interestingly, these values perfectly correlate with the high-pressure methane isotherm described in Figure 7 (magnitude of the first (24%) and second (76%) step). Based on this assumption, one can speculate that sII hydrate promoted by THF grows in the external surface and large pores, taking place in the first step of the high-pressure isotherm, whereas sI structure is associated with gas hydrates grown in the inner pores.

The sII phase was fitted in the space group  $Fd\bar{3}m$  with a unit cell parameter around  $a = 17.3227(3)$ - $17.3685(3)$  Å depending on the temperature, in close agreement with previous sII hydrates reported in the literature [40, 41]. Analysis of the electronic density inside the cages shows that CH<sub>4</sub> occupies the small cages and THF resides in the large cages. THF molecule rotates freely inside the corresponding cavity resulting in almost spherical distribution of the electronic density around the cavity center which was approximated by placing the carbon atoms in the general position (site multiplicity=192) and fixing the molecular geometry.

Attempts of refinement of the CH<sub>4</sub> and THF occupancies did not result in any significant deviation from 1 molecule per cavity. Under these circumstances, the stoichiometry for the sII hydrate would be 0.5 THF·1 CH<sub>4</sub>·8.5H<sub>2</sub>O, in close agreement with the first step in Table 6. In other words, the filling of large cavities by THF limits the amount of methane encapsulated, thus explaining the lower methane uptake in the first step of the isotherm in the presence of THF (Figure 7).

The sI structure present in the PPAC + THF system exhibits similar structural details to the PPAC system with pure water with unit cell parameters ranging from 11.9661(2) to 11.9959(1) Å. However, the filling of the cavities becomes more complex in the presence of an aqueous solution of THF (see Table 8). At -33°C both cavities are almost completely filled (only minor amount of vacancies is observed in the small cavities). Surprisingly, at 2°C intensities of the peaks belonging to the sI phase change significantly reflecting substantial redistribution of the electronic density within the unit cell. The Fourier maps show that the density maxima in both cavity types are split (Figure 11). Also, reasonable agreement between the calculated and experimental diffraction patterns can be only achieved by increasing of the total

number of electrons inside the cavity almost twofold compared to the low-temperature measurements. Overall, the intensities of the diffraction maxima are highly similar to that observed for ethane or acetylene hydrates [44-46].

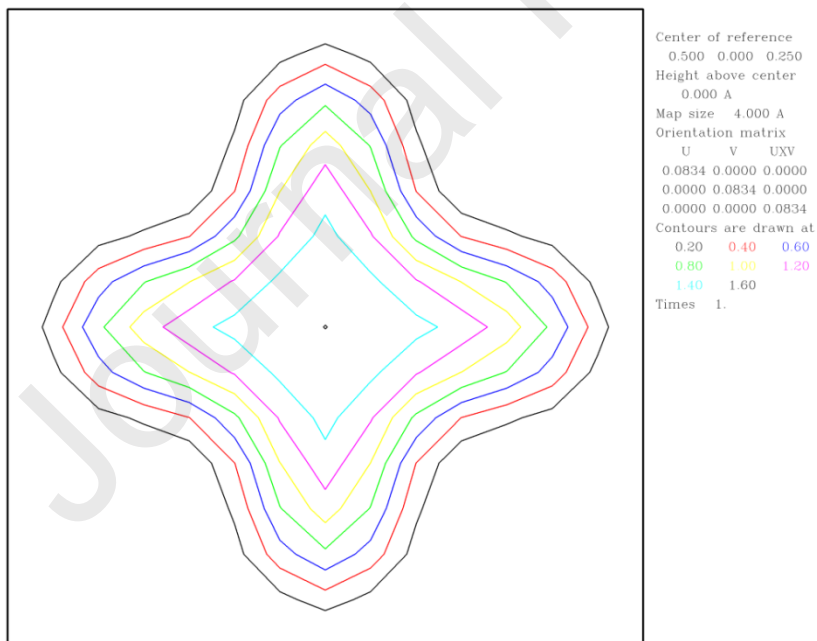
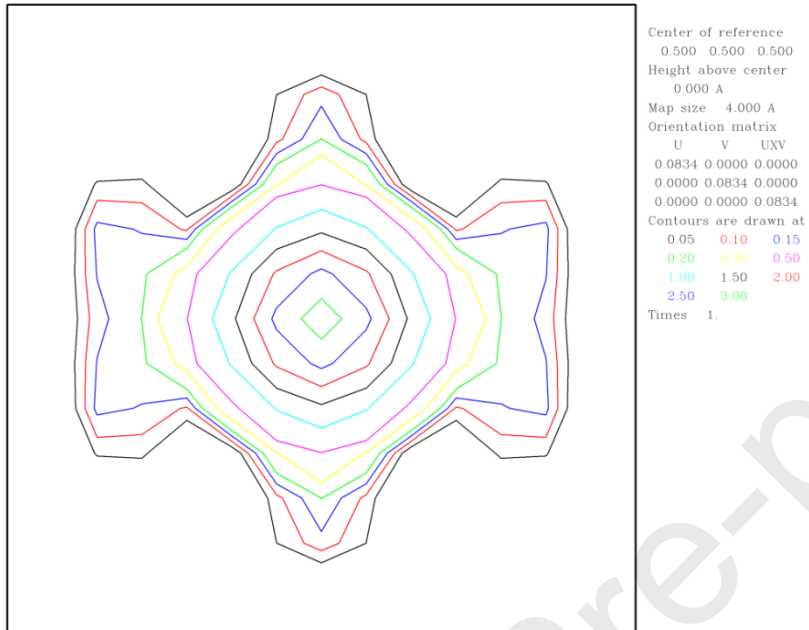


**Figure 11.** Electron density distribution inside small (top) and large (bottom) cavities of the sl phase of PPAC+THF sample at 2°C and 4.0 MPa. The lobes correspond to the positions of C1 and C3 atoms, respectively.

Following the structure model proposed in [46], the sl phase at 2°C was described using two non-equivalent carbon positions in the small cavities (C1 & C2, 6 and 12 equivalent positions within each cavity, respectively) and two non-equivalent carbon positions in the large cavities (C3 & C4, 4 and 2 equivalent positions within each cavity, respectively). After occupancy refinement, total amount of the carbon atoms appeared to be 1.686 in the small cages and 2.498 in the large cages. In other words, the SXRPD data suggest the presence of  $C_2H_x$  species encapsulated in small and large cages, with an occupation of 0.843 and 1.25, respectively. These results are somehow unexpected since sl cavities are assumed to allocate a single carbon atom from each  $CH_4$  molecule. Unfortunately, at this point we do not have a clear explanation for these results and further studies using *in-situ* Raman or NMR would be needed.

To end up, it is important to highlight that the variation of the crystal size between the measurements supports the conclusion about the strong kinetical limitations on formation of the methane hydrate without additives. In case of the PPAC sample the particle size of the methane hydrate kept increasing during the whole experiment ranging from 80 nm at -33°C to 215 nm at 2°C. On the other hand, for the PPAC+THF sample the size of the methane hydrate crystals remains essentially unchanged throughout the experiment meaning that the formation of the methane hydrate particles was completed already after the first few minutes of pressurization.

**Table 8.** Structural parameters for sl and sII structure in sample PPAC pre-adsorbed with H<sub>2</sub>O + THF (P<sub>CH<sub>4</sub></sub> = 4.0 MPa).

Sample	Temperature, C	sl phase					sII phase				
		a, Å	$\theta_{SC}$ (5 <sup>12</sup> )	$\theta_{LC}$ (5 <sup>12</sup> 6 <sup>2</sup> )	wt %	size, nm	a, Å	$\theta_{SC}$ (5 <sup>12</sup> )	$\theta_{LC}$ (5 <sup>12</sup> 6 <sup>4</sup> )	wt %	size, nm
PPAC + H <sub>2</sub> O+ THF+CH <sub>4</sub>	-33	11.9661(2)	methane 0.95(2)	methane 1 (not refined)	74.9	282	17.3227(3)	methane 1 (not refined)	THF 1 (not refined)	25.1	167
PPAC + H <sub>2</sub> O+ THF+CH <sub>4</sub>	2	11.9959(1)	C1: 0.131(7) C2: 0.075(2) Overall C in cage 1.686	C3: 0.435(4) C4: 0.379(5) Overall C in cage 2.498	75.4	240	17.3685(3)	methane 1 (not refined)	THF 1 (not refined)	24.6	158

## Conclusions

A high-surface area activated carbon material has been used as a host structure to promote the nucleation and growth of methane hydrates after the incorporation of organic additives. Organic additives have been incorporated either dissolved in the pre-adsorption media (ultrapure water) or anchored to the carbon surface through a mechanochemical approach. Experimental results show that the mechanochemical approach does not allow to improve the storage performance due to the steric restrictions of the bulkier organic groups. On the contrary, the incorporation of the additives dissolved in water give rise to a promotion in the nucleation and growth kinetics (preferentially for SDS) and a promotion in the thermodynamics (in the specific case of THF). Synchrotron XRPD analysis anticipates a pure sl structure in the PPAC system with water, whereas a combination of sl and sII structures is anticipated in the PPAC system with water+THF. Contrary to bulk hydrates, sl structure in confined hydrates exhibit a preferential occupation for small cages, while larger cages remain only partially occupied. The occupation decreases with temperature, mainly for larger cages.

## Acknowledgement

The authors would like to acknowledge financial support from the MINECO (MAT2016-80285-p), Generalitat Valenciana (PROMETEOII/2014/004), H2020 (MSCA-RISE-2016/NanoMed Project), and Spanish ALBA synchrotron (Projects 2019023322).

## 4. References

1. S. Thomas, R.A. Dawe, Review of ways to transport natural gas energy from countries which do not need the gas for domestic use, *Energy*, 28 (2003) 1461-1477.
2. A. Thiruvengadam, M. Besch, V. Padmanaban, S. Pradhan, B. Demirgok, Natural gas vehicles in heavy-duty transportation-A review, *Energy Policy*, 122 (2018) 253-259.

3. Rodríguez-Reinoso, F. and J. Silvestre-Albero, *Methane Storage on Nanoporous Carbons, in Nanoporous Materials for Gas Storage*, K. Kaneko and F. Rodríguez-Reinoso, Eds. (2019) Springer Singapore: Singapore. p. 209-226.
4. Y. He, W. Zhou, G. Qian, B. Chen, Methane storage in metal–organic frameworks, *Chem. Soc. Rev.*, 43 (2014) 5657-5678.
5. Y. Peng, V. Krungleviciute, I. Eryazici, J.T. Hupp, O.K. Farha, and T. Yildirim, Methane Storage in Metal–Organic Frameworks: Current Records, Surprise Findings, and Challenges, *J. Am. Chem. Soc.*, 135 (2013) 11887-11894.
6. H. Marsh, F. Rodríguez-Reinoso, *Chapter 2 - Activated Carbon (Origins)*, in *Activated Carbon*, H. Marsh and F. Rodríguez-Reinoso, Ed. (2006) Elsevier Science Ltd: Oxford. p. 13-86.
7. M.E. Casco, M. Martínez-Escandell, E. Gadea-Ramos, K. Kaneko, J. Silvestre-Albero, and F. Rodríguez-Reinoso, High-Pressure Methane Storage in Porous Materials: Are Carbon Materials in the Pole Position?, *Chem. Mater.*, 27 (2015) 959-964.
8. T. Tian, Z. Zeng, D. Vulpe, M.E. Casco, G. Divitini, P.A. Midgley, J. Silvestre-Albero, J.-C. Tan, P.Z. Moghadam, and D. Fairen-Jimenez, A sol–gel monolithic metal–organic framework with enhanced methane uptake, *Nature Materials*, 17 (2018) 174-179.
9. B.M. Connolly, M. Aragonés-Anglada, J. Gandara-Loe, N.A. Danaf, D.C. Lamb, J.P. Mehta, D. Vulpe, S. Wuttke, J. Silvestre-Albero, P.Z. Moghadam, A.E.H. Wheatley, and D. Fairen-Jimenez, Tuning porosity in macroscopic monolithic metal-organic frameworks for exceptional natural gas storage, *Nature Communications*, 10 (2019) 2345.
10. E.D. Sloan, Fundamental principles and applications of natural gas hydrates, *Nature Communications*, 426 (2003) 353-359.
11. C.A. Koh, E.D. Sloan, A.K. Sum, D.T. Wu, Fundamentals and Applications of Gas Hydrates. *Annu. Rev. Chem. Biomol. Eng.*, 2 (2011) 237-257.
12. E.D. Sloan and C.A. Koh, *Clathrate hydrates of natural gases, 3<sup>rd</sup> Ed.* (2007) 1-730.
13. P. Englezos, Clathrate hydrates, *Ind. Eng. Chem. Res.*, 32 (1993) 1251-1274.
14. D. Daniel-David, F. Guerton. C. Dicharry, J.-P. Torré, D. Broseta, Hydrate growth at the interface between water and pure or mixed CO<sub>2</sub>/CH<sub>4</sub> gases: Influence of pressure, temperature, gas composition and water-soluble surfactants, *Chem. Eng. J.*, 132 (2015) 118-127.
15. N.-J. Kim, J. Hwan Lee, Y.S. Cho, W. Chun, Formation enhancement of methane hydrate for natural gas transport and storage, *Energy*, 35 (2010) 2717-2722.
16. Y. He, M.-T. Sun, C. Chen, G.-D. Zhang, K. Chao, Y. Lin, F. Wang, Surfactant-based promotion to gas hydrate formation for energy storage, *J. Mater. Chem. A*, 7 (2019) 21634-21661.
17. A. Kumar, O.S. Kushwaha, P. Rangsunvigit, P. Linga, R. Kumar, Effect of additives on formation and decomposition kinetics of methane clathrate hydrates: Application in energy storage and transportation, *Canadian J. Chem. Eng.*, 94 (2016) 2160-2167.
18. H. Ganji, M. Manteghian, K. Sadaghiani zadeh, M.R. Omidkhah, H. Rahimi Mofrad, Effect of different surfactants on methane hydrate formation rate, stability and storage capacity, *Fuel*, 86 (2007) 434-441.
19. Y. Zhong, R.E. Rogers, Surfactant effects on gas hydrate formation, *Chem. Eng. J.*, 55 (2000) 4175-4187.
20. H. P. Veluswamy, A. Kumar, R. Kumar, P. Linga, An innovative approach to enhance methane hydrate formation kinetics with leucine for energy storage application, *Appl. Energy*, 188 (2017) 190-199.
21. A. Kumar, S.S. Vedula, R. Kumar, P. Linga, Hydrate phase equilibrium data of mixed methane-tetrahydrofuran hydrates in saline water, *J. Chem. Thermodyn.*, 117 (2018) 2-8.

22. A. Kumar, H.P. Veluswamy, P. Linga, R. Kumar, Molecular level investigations and stability analysis of mixed methane-tetrahydrofuran hydrates: Implications to energy storage, *Fuel*, 236 (2019) 1505-1511.
23. D. Mech, P. Gupta, J.S. Sangwai, Kinetics of methane hydrate formation in an aqueous solution of thermodynamic promoters (THF and TBAB) with and without kinetic promoter (SDS), *J. Natur. Gas Sci. and Eng.* 35 (2016) 1519-1534.
24. M.E. Casco, J. Silvestre-Albero, A. Ramirez-Cuesta, F. Rey, J. Jorda, A. Bansode, A. Urakawa, I. Peral, M. Martinez escandell, K. Kaneko, and F. Rodriguez-Reinoso, Methane hydrate formation in confined nanospace can surpass nature, *Nature Communications*, 6 (2015) 6432.
25. C. Cuadrado-Collados, F. Fauth, I. Such-Basañez, M. Martínez-Escandell, J. Silvestre-Albero, Methane hydrate formation in the confined nanospace of activated carbons in seawater environment, *Microp. Mesop. Mater.*, 255 (2018) 220-225.
26. M.E. Casco, F. Rey, J.L. Jordá, S. Rudić, F. Fauth, M. Martínez-Escandell, F. Rodríguez-Reinoso, E.V. Ramos-Fernández, J. Silvestre-Albero, Paving the way for methane hydrate formation on metal–organic frameworks (MOFs), *Chem. Sci.*, 7 (2016) 3658-3666.
27. E. Andres-Garcia, A. Dikhtiarenko, F. Fauth, J. Silvestre-Albero, E.V. Ramos-Fernández, J. Gascon, A. Corma, F. Kapteijn, Methane hydrates: Nucleation in microporous materials, *Chem. Eng. J.*, 360 (2019) 569-576.
28. H. Kakati, A. Mandal, S. Laik, Effect of SDS/THF on thermodynamic and kinetic properties of formation of hydrate from a mixture of gases (CH<sub>4</sub>+C<sub>2</sub>H<sub>6</sub>+C<sub>3</sub>H<sub>8</sub>) for storing gas as hydrate, *J. Energy Chem.*, 25 (2016) 409-417.
29. M.E. Casco, M. Martinez-Escandell, K. Kaneko, J. Silvestre-Albero, F. Rodríguez Reinoso, Very high methane uptake on activated carbons prepared from mesophase pitch: A compromise between microporosity and bulk density, *Carbon*, 93 (2015) 11-21.
30. F. Rodríguez-Reinoso, C. Almansa, M. Molina-Sabio, Contribution to the Evaluation of Density of Methane Adsorbed on Activated Carbon, *J. Phys. Chem. B*, 109 (2005) 20227-20231.
31. A. Vysniauskas, P.R. Bishnoi, A kinetic study of methane hydrate formation, *Chem. Eng. Sci.*, 38 (1983) 1061-1072.
32. J.H. Qiu, T.M. Guo, Kinetics of methane hydrate formation in pure water and inhibitor containing systems, *Chinese J. Chem. Eng.*, 10 (2002) 316-322.
33. T.D. Brown, C.E. Taylor, M.P. Bernardo, Rapid gas hydrate formation processes: Will they work?, *Energies* 3 (2010), 3, 1154-1175.
34. L. Borchardt, W. Nickel, M. Casco, I. Senkovska, V. Bon, D. Wallacher, N. Grimm, S. Krause, J. Silvestre-Albero, Illuminating solid gas storage in confined spaces – methane hydrate formation in porous model carbons, *Phys. Chem. Chem. Phys.*, 18 (2016) 20607-20614.
35. C. Cuadrado-Collados, A.A.A. Majid, M. Martínez-Escandell, L.L. Daemen, A. Missyul, C. Koh, J. Silvestre Albero, Freezing/melting of water in the confined nanospace of carbon materials: Effect of an external stimulus, *Carbon* (2019) DOI: 10.1016/j.carbon.2019.10.081.
36. U.S. National Library of Medicine. National Center for Biotechnology Information. PubChem Database. Sodium dodecyl sulfate, CID=3423265, <https://pubchem.ncbi.nlm.nih.gov/compound/Sodium-dodecyl-sulfate>, accessed Oct. 12, 2019.
37. U.S. National Library of Medicine. National Center for Biotechnology Information, PubChem Database. Leucine, CID=6106, <https://pubchem.ncbi.nlm.nih.gov/compound/Leucine>, accessed Oct. 12, 2019.
38. Y. Paul Handa, D. Stupin, Thermodynamic properties and dissociation characteristics of methane and propane hydrates in 70-Å-radius silica gel pores, *J. Phys. Chem.*, 96 (1992) 8599-8603.

39. K.K. Østergaard, R. Anderson, M. Llamedo, B. Tohidi, Hydrate phase equilibria in porous media: effect of pore size and salinity, *Terra Nova*, 14 (2002) 307-312.
40. J. Shu, X. Chen, I.M. Chou, W. Yang, J. Hu, R.J. Hemley, H.-k. Mao, Structural stability of methane hydrate at high pressures, *Geoscience Frontiers*, 2 (2011) 93-100.
41. Q. Junfeng, C.D. Hartmann, W.F. Kuhs, Cage occupancies of methane hydrates: Results from synchrotron X-ray diffraction and Raman spectroscopy, *Proceedings of the 8th International Conference on Gas Hydrates (ICGH8-2014)*, 2014.
42. J.B. Klauda, S. I. Sandler, Phase behavior of clathrate hydrates: a model for single and multiple gas component hydrates, *Chem. Eng. Sci.*, 58 (2003) 27-41.
43. C.Y. Jones, S.L. Marshall, B.C. Chakoumakos, C.J. Rawn, Y. Ishii, Structure and Thermal Expansivity of Tetrahydrofuran Deuterate Determined by Neutron Powder Diffraction, *J. Phys. Chem. B*, 107 (2003) 6026-6031.
44. K. Morita, S. Nakano, K. Ohgaki, Structure and stability of ethane hydrate crystal, *Fluid Phase Equilibria*, 169 (2000) 167-175.
45. K.A. Udachin, C.I. Ratcliffe, J.A. Ripmeester, Single Crystal Diffraction Studies of Structure I, II and H Hydrates: Structure, Cage Occupancy and Composition, *J. Supramol. Chem.*, 2 (2002) 405-408.
46. M.T. Kirchner, R. Boese, W.E. Billups, L.R. Norman, Gas Hydrate Single-Crystal Structure Analyses, *J. Am. Chem. Soc.*, 126 (2004) 9407-9412.

#### Highlights

- Incorporation of additives to confined hydrates promotes nucleation kinetics.
- Thermodynamics can also be promoted in the specific case of THF.
- Confined gas hydrates exhibit an anomalous occupation of small and large cages.
- THF promotes the sII structure in large pores and sI in narrow cavities.